International Journal of Concrete Structures and Materials

RESEARCH Open Access

Mass Concrete Placement of the Offshore Wind Turbine Foundation: A Statistical Approach to Optimize the Use of Fly Ash and Silica Fume

Mien Van Tran[1,2*] and Vinh Ngoc Chau[1]

Abstract

The experimental program investigated concrete with a large amount of fly ash (FA) with silica fume (SF) to replace Portland cement on the results of semi-adiabatic test, compressive strength test, and the rapid chloride permeability test (RCPT). The replacement ratios of cement by a combination of FA and SF were 30%, 35%, and 40% by mass. The percentages of SF to replace cement were 0%, 4%, and 8% by mass. Three different water-to-binder ratios (W/B) of 0.34, 0.36, and 0.38 were also investigated. Multiple linear regression was applied to construct the predicted equations (models) for the semi-adiabatic temperature rise test and the compressive strength test. Models were assessed statistically and were used to solve the concrete mixture design optimization problems. The mixture with W/B of 0.36, 31% FA, and 5% SF was found to optimally satisfy the multi-objective problem: 28-day compressive strength of 50 MPa, low heat of hydration, and very low chloride penetrability classification. Field test on the actual wind turbine foundation of the optimal mixture revealed the maximum temperature rise was 74.8 °C and the maximum temperature differential was 21.9 °C.

Keywords: mass concrete, fly ash, silica fume, semi-adiabatic, regression analysis

1 Introduction

In Vietnam, the offshore wind turbine foundation is mainly made of slab combined with pile system. The slab foundation for wind turbines is almost exclusively made of reinforced concrete and is a huge structure to resist the massive overturning moment. A typical wind turbine with a capacity from 1 to 2 MW needs approximately 130 to 240 m^3 concrete for the foundation (Berndt, 2004). Because of the low thermal conductivity, massive concrete structures, in their curing time, cannot dissipate the heat of cement hydration efficiently. The accumulation of heat inside the structure leads to huge surface–interior temperature differences, which induce thermal tensile stresses. Furthermore, temperature fluctuation due to the air or water environment may cause extensive tensile stresses to massive structures (Bofang, 2014). Consequently, unwanted thermal cracking appears when the tensile stresses exceed the concrete tensile strength. Those cracks can be severe and destroy the structure's stability and integrity or decrease concrete durability by allowing the penetration of harmful chemical compounds into reinforced concrete. Therefore, it is essential to alleviate thermal cracking risk by reducing the concrete structure's accumulated heat.

Hydration of Portland cement is an exothermic reaction; the heat of hydration of cement liberates the energy up to 120 cal/g (Neville, 1997). According to the Portland Cement Association, every 100 kg of cement in the mix

*Correspondence: tvmien@hcmut.edu.vn
[1] Faculty of Civil Engineering, Ho Chi Minh City University of Technology (HCMUT), 268 Ly Thuong Kiet Street, District 10, Ho Chi Minh City 70000, Vietnam
Full list of author information is available at the end of the article
Journal information: ISSN 1976-0485 / eISSN 2234-1315

proportion increases the maximum temperature rise to 12 °C above the initial concrete temperature after casting (Riding et al., 2006). This calculation is appropriate for concrete containing ASTM C 150 Type 1 cement from 300 to 600 kg/m^3 and assumes that the least dimension of the concrete member is at least 1.8 m. Thus, it is clear to attribute the temperature rise during the curing stage of concrete to the amount of cement being used in the concrete mix proportion. Fly ash (FA), a by-product of burning pulverized coal in thermal power plants, has been used to partially replace Portland cement in the concrete industry for long history. This application benefits the reduction of CO_2 emissions from cement production and provides a solution for FA's disposal. For massive structures such as dams and foundations, high replacement levels (from 30 to 50%) of cement by class F FA are recommended to control temperature rise. However, in Vietnam, the substitution rate of class F FA for Portland cement in concrete production is generally at a low level (below 20%). Compared to the ASTM C618 (2012), the chemical requirements of class F FA in Vietnam Standard, TCVN 10302 (2014), are the same except that the Vietnam Standard allows the loss of ignition (LOI) in class F FA to reach the maximum value of 12%. The residual carbon in high LOI FA can absorb water and chemical admixtures, reducing their efficiency when using in concrete (Pedersen et al., 2008). These days, the quality of class F FA in Vietnam is further improved, with the LOI ranging from 6 to 8%.

There are numerous studies about reducing the hydration heat by partially replacing cement with supplementary cementitious materials (SCMs). Rashad (2015) reviewed Class F FA's effect on the heat of hydration from previous studies (see Table 1) when using it as cement replacement. Class F FA shows little or no hydraulic properties; it helps to reduce the heat of hydration and significantly enhances the concrete's late strength by its pozzolanic properties. However, the low degree of hydration in concrete containing a large FA volume will adversely affect the concrete early age strength. In practice, silica fume (SF) is commonly used in concrete containing high volume FA to enhance the concrete compressive strength. Imam et al. (2018) reviewed that SF's percentage replacing cement in the range of 8–12% significantly increased the concrete compressive strength. In the study of Gesoğlu et al. (2009), the compressive strength at 90 days of concrete containing the combination of 45% of FA and 15% of SF as cement replacement is 5.65% greater than that of the concrete mixture containing 60% FA as cement replacement. Shaikh et al. (2015) reported using SF at 5% and 10% to replace cement enhanced 7-day compressive strength of high volume FA concrete by about 5 and 6%, respectively.

Besides thermal damage, concrete durability should also be carefully considered as slab foundation for the offshore wind turbine is often placed in the tidal or splash zones. These zones provide many transportation mechanisms of aggressive species into concrete structures, such as diffusion, sorption, permeation, abrasion, and erosion (Santhanam & Otieno, 2016). Reinforced concrete exposed to the marine environment must perform good resistance to corrosion and chemical attacks caused by the high concentration of chlorides and sulfates. Thomas (2016) stated that the rate of diffusion of chlorides depends on the pore structure, and the physical resistance to chloride penetration could be enhanced if the pore system inside the concrete structure is small and disconnected from each other. Holland et al. (2016) stated that, in many research, the diffusion coefficient of FA concrete is similar to that of plain cement concrete at early ages. But at later ages, the use of FA does result in a lower diffusion coefficient than that of plain cement concrete. Boğa and Topçu (2012) concluded that the use of FA at 15, 30, and 45% to replace cement significantly reduces the chloride permeability compared to the mixture with no FA content. Chalee et al. (2010) investigated FA from 0 to 50% in concrete and found that the increase in FA content reduced the chloride penetration and steel corrosion in concrete. Meanwhile, SF reacted quickly and resulted in a smaller diffusion coefficient at all ages compared with those of plain cement concrete. Bentz (2000) investigated the effect of SF, from 0 to 10%, on the diffusion coefficient of concrete and found that the diffusion coefficient decreased in accordance with the increase in the percentage of SF. Besides the physical resistance to the chloride penetration, the appropriate dosage of SCMs helps to increase the chloride binding capacity of the hydrated phases. Thomas et al. (2012) tested the chloride

Table 1 Summary of previous studies about the effect of FA on the heat of hydration.

References	FA content (%)	Effect
Poon et al. (2000)	45	Reducing the heat of hydration by 36%
Li (2004)	50	Reduction in the heat of hydration
Yoshitake et al. (2013)	50	Reducing the adiabatic temperature rise by 40%
Duràn-Herrera et al. (2011)	45, 60, 75	Reducing the semi-adiabatic peak temperature significantly

binding of the hydrated cement paste containing different types of SCMs and found that the high content of alumina (Al_2O_3) in metakaolin, FA, and slag increased the chloride binding. The chloride binding has a significant effect on the reduction of chloride penetration as the availability of free chloride is also reduced by the binding mechanism, and the effect on the time of corrosion initiation as the reduction in free chloride helps to reduce the concentration of chloride ions near the steel reinforcement (Martín-Pérez et al., 2000).

In many aspects, the combination of SF and FA works better than either material alone. Compared with mixtures with only FA, the mixture with FA combined with SF significantly reduced the water absorption and sorptivity (Leung et al., 2016). Chu et al. (2019) conducted an experimental program to evaluate the properties of the mixture containing 0–30% FA and 0–10% SF used as cement replacement. The testing methods consisted of the permeability of chloride and sulfate ions, microstructural analysis, and field experiments by producing the sea dykes and testing them on the Vietnam coast. They concluded that the best-performing mixture contained 20% FA and 10% SF. However, Ghosh and Tran (2015) conducted a comprehensive study on binary and ternary mixtures to investigate the long-term resistance against corrosion; they found that although most ternary mixtures have substantial influence to increase the electrical resistivity, the compatibility of Class C FA with other SCMs (e.g., SF) was not good which resulted in the unsatisfactory in term of the development of electrical resistivity. Using SF in mass concrete may also bring the shortcoming of preventing thermal damages. SF is a very reactive pozzolanic material as it has high amorphous silicon dioxide content. The pozzolanic reaction of SF rapidly consumes the Portlandite, a by-product of Portland cement hydration, and liberates energy. Kadri and Duval (2009) reported that the cumulative hydration heat of concrete containing 10% SF as cement replacement was higher than that of reference concrete using ternary blended cement containing FA and SF. In mass concrete placement, the use of SF should be optimized to reduce the heat of hydration for avoiding thermal damages and producing economic concrete as SF is an expensive material.

Attempts have been made to evaluate the applicability of SCMs using cement replacement to reduce the temperature rise in mass concrete structures. Researchers from Japan and Singapore investigated the thermal characteristic of concrete containing FA and blast-furnace slag (BFS) by measuring the temperature rise in adiabatic conditions and mock-up specimens. Three concrete mixes were investigated; the mix with 14% FA and 55% BFS exhibited the least temperature rise. Two other mixes using 30% FA alone and 65% BFS alone showed higher results in temperature rise. However, in order to simulate the adiabatic condition, tested specimens had to be large in volume with at least a dimension of 1.5 m in mock-up test (Tada et al., 2016) or the 50 l concrete samples in adiabatic test (Mitani et al., 2016). Consequently, only a few concrete mix designs could be investigated. It was not easy to optimize the mixture proportion by conducting a full factorial experimental program as the cost for this kind of project will be prohibitively expensive.

This manuscript provides a detailed approach to optimize the concrete mixture proportion for mass concrete placement of the actual construction of the wind turbine foundation located in Vietnam. The project required the consultation of appropriate concrete mixture proportions to alleviate thermal damage due to mass pouring in hot weather conditions and real-time monitoring of temperature rise when constructing the foundation. The first step was to point out the optimal combination between cement, FA, and SF from the laboratory point of view. Laboratory tests such as compressive strength, the temperature rise of concrete in semi-adiabatic conditions, and rapid chloride permeability test (RCPT) have been carried. The results were analyzed statistically, and an optimal mixture was determined and practically used for the actual construction of the slab foundation of an offshore wind turbine. Then the practical result of temperature rise monitoring of the pouring placement was also presented.

2 Experimental Investigation

2.1 Materials

The experimental study was carried out on concrete with Class-F FA, and SF used as cement replacement. The chemical analyses of SCMs used in this study are presented in Table 2. The cement used in this study was the ordinary Portland cement (OPC). Crushed stone

Table 2 Chemical analysis of SCMs.

Chemical analysis (%)	Fly ash (FA)	Silica fume (SF)
SiO_2	55.7	93.4
Al_2O_3	23.4	0.45
Fe_2O_3	6	0.25
CaO	0.02	–
MgO	1	0.79
SO_3	0.07	0.46
K_2O	3.77	1.27
Na_2O	–	0.61
C	2.98	0.45
Loss on ignition	7	2

with maximum particle sizes (D_{max}) of 20 mm, classified according to the TCVN 7572 (2006), was used as conventional coarse aggregate. Crushed sand and river sand were used as fine aggregates. A poly(carboxylate ether)-based superplasticizer with a specific gravity of 1.04 was used with a dosage of 1.3% by the total amount of cementitious materials to prevent slump loss and extend the setting time of concrete. All concrete mixtures are shown in Table 3.

2.2 A Statistical Approach to Optimize the Mix Proportion

In multiple linear regression, the objective would be to develop a prediction equation that expresses the outcomes as a function of several independent variables. In this study, the outcomes that would be predicted were the results of the semi-adiabatic test and the compressive strength test. The independent variables were the content of Portland cement, Class-F FA and SF. These independent variables (or factors) were presented as a 3^3 full factorial experiment (see Table 4), which means three independent variables are considered, each at three levels. The reliability of the prediction equations would be statistically assessed to decide which model should be chosen as an objective function in the optimization problem.

Table 4 The test program of this study.

Level	Factors		
	Binder (kg/m^3) (x_1)	Fly ash and silica fume (% by weight) (x_2)	Silica fume (% by weight) (x_3)
1	431	40	0
2	411	35	4
3	391	30	8

Table 3 Concrete mixture proportioning.

Mix no.	Binder kg/m^3	FA + SF kg/m^3 (%)	SF kg/m^3 (%)	Water kg/m^3	River sand kg/m^3	Crushed sand kg/m^3	Coarse aggregate kg/m^3	Superplasticizer l/m^3
1	431	129.3 (30)	0 (0)	147.5	363.2	484.2	973.9	5.6
2	431	150.8 (35)	0 (0)	147.5	361.8	482.4	970.2	5.6
3	431	172.4 (40)	0 (0)	147.5	360.4	480.5	966.5	5.6
4	431	129.3 (30)	17.2 (4)	147.5	363.2	484.2	973.9	5.6
5	431	150.8 (35)	17.2 (4)	147.5	361.8	482.4	970.2	5.6
6	431	172.4 (40)	17.2 (4)	147.5	360.4	480.5	966.5	5.6
7	431	129.3 (30)	34.5 (8)	147.5	363.2	484.2	973.9	5.6
8	431	150.8 (35)	34.5 (8)	147.5	361.8	482.4	970.2	5.6
9	431	172.4 (40)	34.5 (8)	147.5	360.4	480.5	966.5	5.6
10	411	123.3 (30)	0 (0)	147.5	366.3	488.4	982.3	5.34
11	411	143.8 (35)	0 (0)	147.5	365.0	486.4	978.8	5.34
12	411	164.4 (40)	0 (0)	147.5	363.7	484.9	975.3	5.34
13	411	123.3 (30)	16.4 (4)	147.5	366.3	488.4	982.3	5.34
14	411	143.8 (35)	16.4 (4)	147.5	365.0	486.4	978.8	5.34
15	411	164.4 (40)	16.4 (4)	147.5	363.7	484.9	975.3	5.34
16	411	123.3 (30)	32.9 (8)	147.5	366.3	488.4	982.3	5.34
17	411	143.8 (35)	32.9 (8)	147.5	365.0	486.4	978.8	5.34
18	411	164.4 (40)	32.9 (8)	147.5	363.7	484.9	975.3	5.34
19	391	117.3 (30)	0 (0)	147.5	369.9	493.2	991.9	5.08
20	391	136.8 (35)	0 (0)	147.5	368.6	491.5	988.5	5.08
21	391	156.4 (40)	0 (0)	147.5	367.4	489.8	985.2	5.08
22	391	117.3 (30)	15.6 (4)	147.5	369.9	493.2	991.9	5.08
23	391	136.8 (35)	15.6 (4)	147.5	368.6	491.5	988.5	5.08
24	391	156.4 (40)	15.6 (4)	147.5	367.4	489.8	985.2	5.08
25	391	117.3 (30)	31.3 (8)	147.5	369.9	493.2	991.9	5.08
26	391	136.8 (35)	31.3 (8)	147.5	368.6	491.5	988.5	5.08
27	391	156.4 (40)	31.3 (8)	147.5	367.4	489.8	985.2	5.08

The techniques that are mainly used to construct the multiple linear regression models presented in this manuscript are based on the work of Mendenhall and Sincich (2016), "*Statistics for engineering and the sciences*". Eq. (1) presents the first-order model, which is the most basic multiple linear regression model encountered in practice, with three quantitative independent variables, x_1, x_2, x_3 (see Table 4). β_0 is the y-intercept, β_i represents the regression coefficient relating to x_i when all other x's are held fixed, which means the value of β_i showed the weight of contribution of each constituent (x_i) in the concrete mixture design on the outcome properties. The $E(y)$ is the outcome (the semi-adiabatic temperature rise, the compressive strength) that would be predicted. The first-order model assumes that there is "no interaction" among the independent variables, which means the effect of changes in one variable (say, x_1) on the outcome $E(y)$ is the same regardless of the value of the others (say, x_2, x_3). That is to say, the effect of each independent variable on the outcome is totally separate from other independent variables. Thus, the outcome is just the result of simply accumulating all the effects of every independent variable:

$$E(y) = \beta_0 + \beta_1 x_1 + \beta_2 x_2 + \beta_3 x_3. \quad (1)$$

In the multiple regression model, multicollinearity refers to the condition that there is an occurrence of high intercorrelations among the independent variables (x_1, x_2, x_3). It leads to the difficulty of distinguishing the individual effects of independent variables on the dependent variable ($E(y)$) because the values of one independent variable can be derived from other independent variables. Fig. 1 provides the correlation plots of independent variables in pairs. There is no evidence of a heavy correlation between any pair in the data because the investigation is conducted in a full factorial design of experiments. Hence, multicollinearity can be safely ignored in this research as there is no ability to determine the value of an independent variable by using the value of other independent variables.

Valid inferences about β_i depend on the probability distribution of random error (ε). Therefore, some specific assumptions must be made to the statistical regression analysis:

- Assumption 1: The mean of ε is 0. (Linearity)
- Assumption 2: The variance of ε is equal to a constant for all values of x_i. (Homoscedasticity)
- Assumption 3: The probability distribution of ε is normal. (Normality)
- Assumption 4: The random error is independent. (Statistical independent)

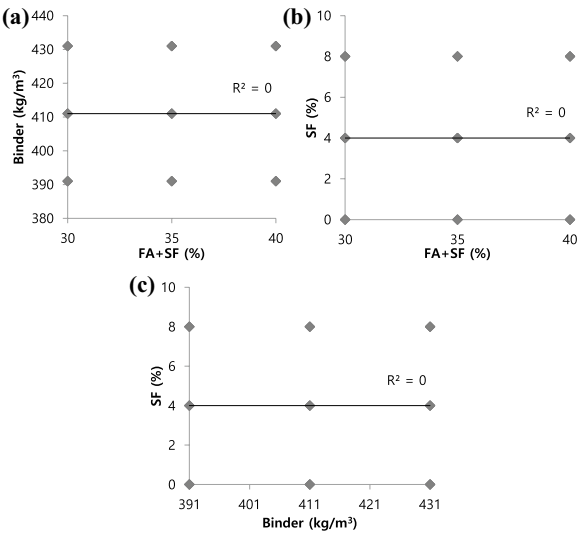

Fig. 1 Correlation plots for validating the independence of independent variables (**a** binder (x_1) versus FA + SF (x_2), **b** FA + SF (x_2) versus SF (x_3), **c** binder (x_1) versus SF(x_3)).

Although it is difficult for these assumptions to be satisfied precisely in the practical application, gross violations from these assumptions will lead to unreliable results. In this manuscript, regression residual was applied to check these assumptions. As a residual is an estimation of the true error of prediction for a particular observation, it provides information on the validity of the assumptions:

$$\text{Residual} = y - y_{\text{est}}, \quad (2)$$

where y is an observed value, and y_{est} is an estimated value.

A summary of the steps to constructing the multiple linear regression model is as follows:

- Apply the multiple linear regression using the EXCEL software to build models (e.g., compressive strength, semi-adiabatic temperature rise) as functions of independent variables.
- Check the utility of models. EXCEL software generates the printout sheet of multiple linear regression analysis containing the analysis of variance F test and the T test on the individual β parameters. The F test will be used to test the overall adequacy of the model, and T tests examine the statistical significance of the corresponding independent variable. All the tests are assessed by the p-value. A p-value of 5% or less is a generally accepted point at which to reject the null hypothesis and demonstrate how confident the model is statistically helpful in predicting the targeted outcome. For the β_0, it will not have a meaningful interpretation unless it makes sense to set the

values of all independent variables (x_1, x_2, x_3) simultaneously equal 0 (Mendenhall & Sincich, 2016). In this study, because x_1, x_2, and x_3 cannot simultaneously equal 0 (binder cannot equal 0 kg/m^3), the y-intercept is meaningless, and the hypothesis testing for the β_0 can be ignored.

– Check the four assumptions by using residual regression.
– If the model is deemed adequate and the assumptions are satisfied, it can be used as an objective function and predict the outcome.

Fig. 2 illustrates the method to obtain the optimal mixture in this study. Experimental data on compressive strength, semi-adiabatic test, and rapid chloride permeability test were collected. Then models of compressive strength and semi-adiabatic test results were constructed based on plausible values of the quantities of binder (kg/m^3), FA + SF (%), SF (%). The utility of models was assessed to determine which model should be the objective function. Concrete properties specifications involved designing concrete compressive strength at 50 MPa with low hydration heat and good performance to chloride permeability resistance. Constraints were determined through the experimental program and the concrete mixture was optimized with EXCEL's support.

2.3 Laboratory Testing Methods

- Compressive strength and semi-adiabatic temperature rise test

A total of 81 cubic concrete specimens ($100 \times 100 \times 100$ mm) for 27 mixtures were prepared (3 replicates for each mixture) to determine the concrete compressive strength. After casting, all specimens were cured in water until the designated test age. The compressive strength of concrete was conducted at the age of the 7th and 28th day.

To measure the concrete temperature rise due to heat of hydration, F-Cal 4000, a commercial semi-adiabatic device manufactured by Calmetrix Inc. (see Fig. 3a), was used to record the temperature rise of all the concrete mixtures. The device has four sample channels and four thermal sensors placed at the bottom of each channel. Surrounding them are thermal insulation layers that prevent heat loss during the test. A logger device records temperature change in each channel every 1 min, and the time–temperature curves are displayed on the computer connected with the semi-adiabatic device by a USB cable (see Fig. 3b). Because the semi-adiabatic measurement is a device that relies only on the insulation layers around the samples to limit the

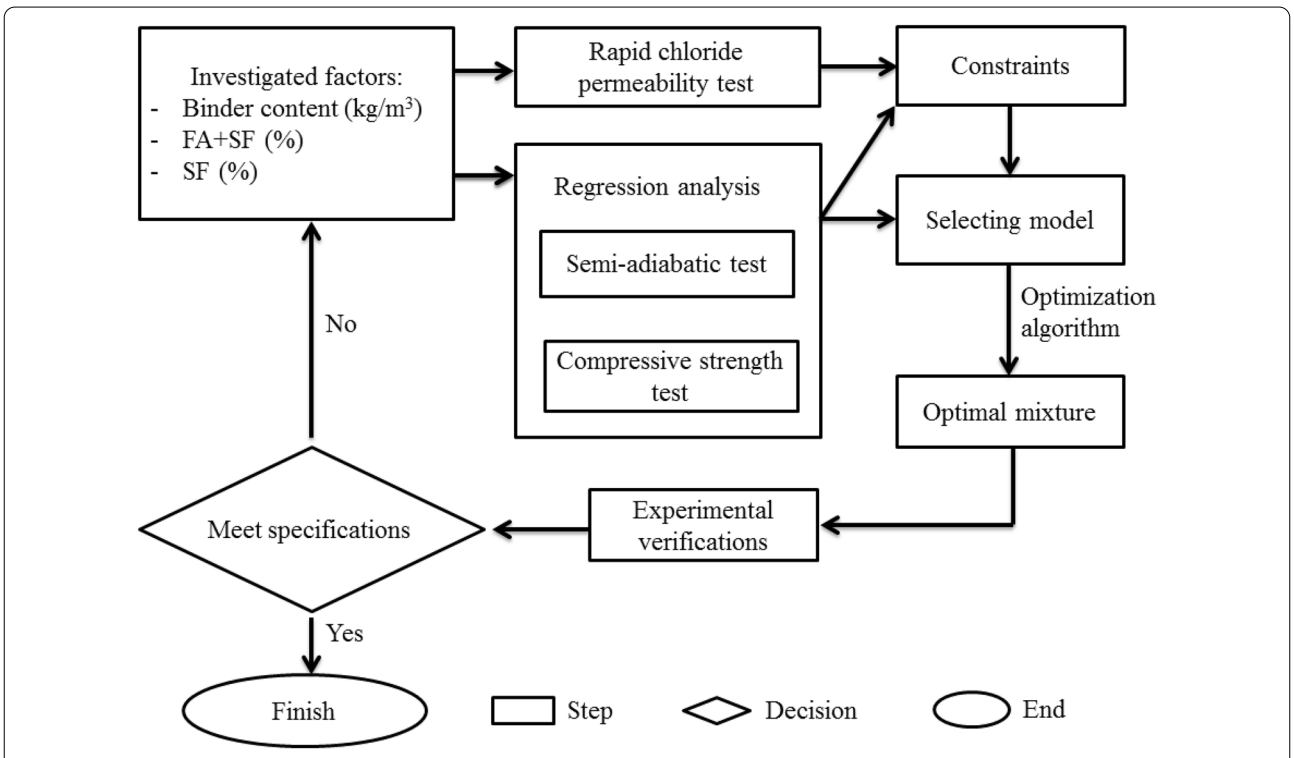

Fig. 2 Flowchart of the concrete proportioning's optimization.

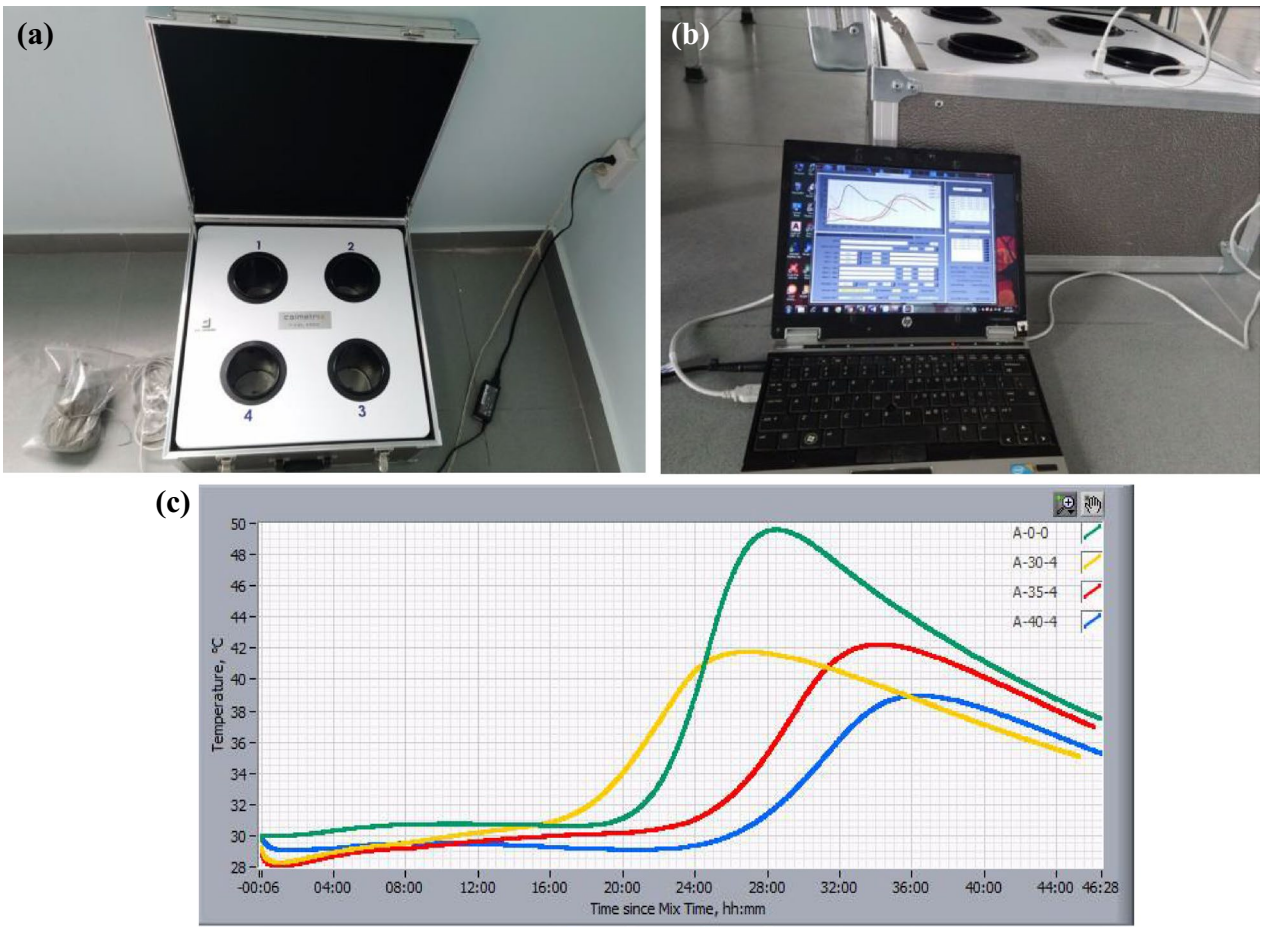

Fig. 3 Semi-adiabatic calorimeter (**a** Fcal-4000 instrument, **b** connecting the Fcal 4000 to the laptop through USB cable, **c** displaying the records of the temperature rise).

heat loss below 100 J/h.K (TCE1 1997), this measurement cannot truly reflect the adiabatic temperature rise. However, some studies focusing on estimating the adiabatic temperature rise using the semi-adiabatic test have demonstrated that the peak temperature in the semi-adiabatic test in concrete and mortar samples can be converted into concrete peak adiabatic temperature rise by an experimental linear equation with high accuracy (Chau et al., 2020; Lee et al., 2018). Besides, the semi-adiabatic test has an advantage: its convenient operation can significantly reduce the testing time.

The fresh concrete would be poured into plastic bags with the same weight of 3 kg for each concrete mix proportion after mixing. The samples were then placed inside the F-Cal 4000 instrument and stored in a room with a constant temperature of 28 °C. The test on average finished after 2 days when the sample already reached its peak of hydration. Graphical data (see Fig. 3c) can be provided with the software's help that goes along with the semi-adiabatic device.

- Rapid chloride permeability test (RCPT)

RCPT (ASTM C1202, 2012) provides the procedure to measure the electrical passing charges (in coulomb) that can indicate permeability of chloride ions through concrete under a potential difference of 60 V. Fig. 4 presents the equipment to conduct the test. After 28 days, cylindrical concrete samples (height: 50 mm, diameter: 100 mm) were sliced from bigger cylindrical samples (height: 200 mm, diameter: 100 mm). The specimens were sealed with epoxy coatings for all sides except two exposed surfaces (top and bottom). After that, the specimens were kept in saturated calcium hydroxide solution for one day and then rinsed with tap water. Next, the specimens were placed in two cells, the cathode cell was filled with 3% sodium chloride, and the anode cell was filled with 0.3 N sodium hydroxide. An external electrical potential energy of 60 V had applied axially across the specimens for 6 h to force the chloride ions outside to migrate into the specimens. The automatic data

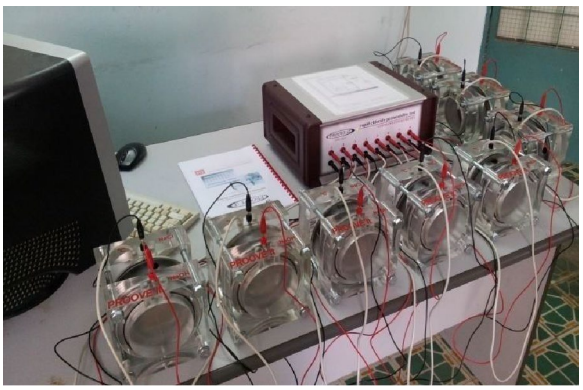

Fig. 4 Rapid chloride permeability test (RCPT) equipment.

processing equipment was used to perform the integration during or after the test and display the coulomb value. The total charge passed is a measure of the concrete's electrical conductance during the test period. In this research, the automatic data processing equipment will collect and display both the current and the coulomb values every 5 min.

2.4 Field Monitoring of the Temperature Rise of the Optimal Mixture

The optimal obtained from this experimental investigation was recommended for constructing the slab foundation of the offshore wind turbine. The construction was completed in 2020 at Tra Vinh province, Vietnam. The size of the mass placement was approximately 22 m in diameter and 3.7 m high. The construction of this mass placement (see Fig. 5) was carried out in the hot weather condition of summer, which means the maximum temperature of the placement could increase dramatically due to the solar radiation absorption. The specifications of this mass concrete placement project involved: the initial temperature of fresh concrete before casting must be below 32 °C, the allowable maximum temperature rise is 75 °C (to prevent the delayed ettringite formation for FA concrete), and the difference of temperature rise between any two locations in the structure must be below 25 °C (to reduce thermal stress). Fig. 6 describes four positions (VT1, VT2, VT3, VT4) that were installed thermal sensors to monitor the temperature of concrete of the wind turbine foundation. Each temperature monitoring position had three thermal sensors: 300 mm from the top concrete surface, the center of the concrete block, and 300 mm from the bottom.

3 Laboratory Results

Results of all performed laboratory tests are presented in Table 5. The test values of 28-day compressive strength varied from 40.8 MPa to 73.6 MPa. Compressive strength at the age of 7 averagely equaled 79% of the 28-day compressive strength. The temperature rise values had the range between 7.64 °C and 13.77 °C, while the time to reach the peak temperature changed from nearly 18 h to around 60 h. The RCPT test measuring total charge passed (coulomb) was performed in two water-to-binder ratios (W/B) series, 0.34 and 0.36. The discussions of the result are presented as follows.

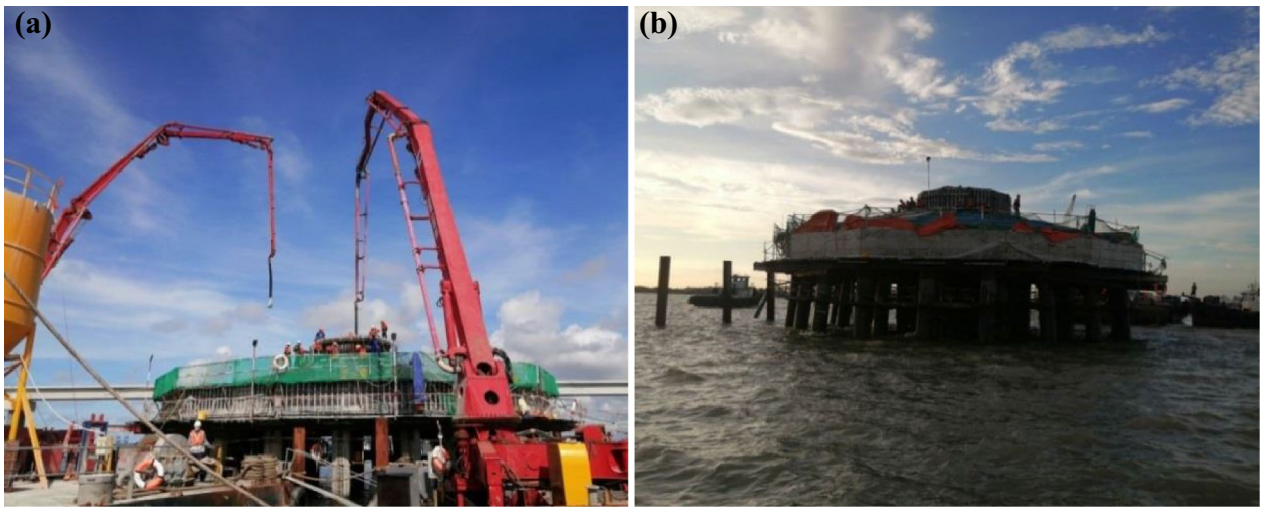

Fig. 5 Mass placement of the offshore wind turbine foundation (**a** Pouring fresh concrete to the foundation, **b** the foundation after 5 days of temperature monitoring).

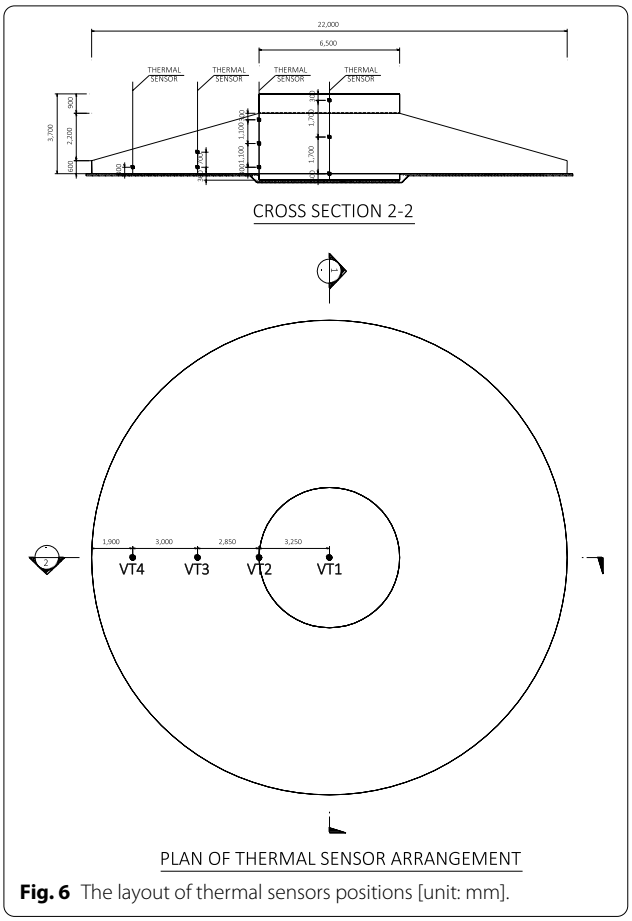

Fig. 6 The layout of thermal sensors positions [unit: mm].

3.1 Temperature Rise in Semi-adiabatic Test

Performing the semi-adiabatic test is to measure the temperature history of different concrete mixtures in the same conditions (volume of sample, heat loss, and curing condition); thereby, the temperature rise profile is generated to display which mix is preferable for concrete mass placement. Furthermore, concrete with class-F FA used as cement replacement can significantly reduce the hydration rate, making the mix incompatible for placement. Hence, the profile of the duration to reach peak temperature is helpful to assess the incompatibility of the concrete mixes. Graphical results of temperature rise in semi-adiabatic conditions are presented for each mixture design as shown in Fig. 8a–c. The temperature rise was measured by subtracting the maximum temperature rise during the hydration period with fresh concrete's initial temperature after mixing (see Fig. 7). With a certain SF level, it was evident that the temperature rise reduced continuously with the increase of SCMs being used as cement replacements. In other words, the higher percentages of FA were used, the lower the temperature rise was achieved. As class F FA has pozzolanic properties and does not show hydraulic properties like cement (ASTM C618, 2012), the results were apparent to understand.

Meanwhile, the effect of SF is clearly illustrated in Fig. 8d–f. The duration time to reach the peak temperature was reduced significantly with SF's increase in replacing the cement. The results can be attributed to the SF's physical effect that provides the nucleation site where the cement hydration product can more readily precipitate from the solution (ACI 234R-06, 2006). Thus, the SF accelerates the rate of hydration in the early ages.

The combination between FA and SF showed much pozzolanic activity in the semi-adiabatic test than did the FA alone as we could observe the mixtures without SF generally showed the lowest temperature rise and prolonged the time to reach the peak temperature. However, the effect of SF on the semi-adiabatic temperature rise was ambiguous. Fig. 8a–c shows that when the FA + SF is fixed at 30%, mixtures with 4% SF experience the highest values of temperature rise. Nevertheless, this finding is not constant when the FA + SF increases to 35% and 40%. ACI 234R-06 (2006) states that the effects of SF on the total amount of heat evolved are contradictory and mentions that the effect of SF on promoting the rate of hydration depends on the Portlandite availability. SF consumes the Portlandite as early as 12 h, and FA reduces the Portlandite content at early ages by delaying its production (Weng et al., 1997). Therefore, the unclear effect of SF on the temperature rise in this study may be attributed to the difference in Portlandite content at early ages among different mixture proportions.

Multiple linear regression analyses were conducted to quantify the influences of the independent variables (binder content, proportion of FA and SF, and proportion of SF) on the semi-test results. EXCEL ran the analyses, and the regression results of temperature rise and time to peak temperature are summarized in Tables 6 and 7, respectively. β_o is the *y*-intercept. β_1, β_2, β_3 are the linear regression coefficients of the independent variables (Binder, FA + SF, SF). The value of β_o in this study does not hold any meaning to interpret the regression results; meanwhile, the values of β_1, β_2, β_3 give an estimation about the mean value of temperature rise (Table 6) and time to reach peak temperature (Table 7). For instance, the $\beta_2 = -0.238$ (°C / %) in Table 6 indicates the mean value of temperature rise to decrease 0.238 (°C) for every 1 (%) increase in the independent variable FA + SF from 30 to 40%, and this factor had the most significant influence on the temperature rise. With the same interpretation, the $\beta_3 = -4.165$ (h/%) in Table 7 far outweighs other linear regression coefficients, which estimates the mean value of time to reach peak temperature to reduce 4.165 (h) for every 1 (%) increase in the factor SF from 0 to 8%. It should be highlighted that all mixtures containing no

Table 5 Results of compressive strength, semi-adiabatic test, and RCPT test.

Mix no.	7-day compressive strength (MPa)	28-day compressive strength (MPa)	Temperature rise (°C)	Time to reach the peak temperature (h)	Charge passed (Coulomb)
1	47.5	59.4	10.46	47.17	1060
2	45.2	57.6	10.42	51.83	988
3	36.2	54.4	7.89	49.73	1396
4	59.9	64.2	13.77	29.18	925
5	52.5	60.2	10.64	27.90	689
6	46.8	58.2	8.95	35.90	934
7	60.4	73.6	12.02	22.27	837
8	53.4	65.8	9.67	20.01	522
9	51.9	67.5	8.73	20.62	1013
10	41.4	57.2	11.01	51.40	1480
11	36.3	49.8	10.05	53.45	1216
12	36.1	40.8	9.21	54.58	1548
13	50.9	59.1	11.96	30.18	1120
14	47.5	55.2	10.15	29.01	988
15	40.9	45.9	9.54	31.52	1092
16	59.0	62.8	11.12	20.58	924
17	54.9	60.0	10.74	18.43	760
18	49.6	54.5	9.34	19.27	953
19	36.9	49.5	9.39	55.73	–
20	34.2	45.6	8.59	58.89	–
21	32.4	41.1	8.58	59.90	–
22	42.1	60.1	10.39	24.63	–
23	36.7	55.1	8.81	25.30	–
24	30.8	50.6	7.64	26.73	–
25	42.3	57.4	9.93	19.18	–
26	41.1	56.6	9.52	21.01	–
27	38.3	45.9	8.73	21.48	–

SF prolonged the duration to reach the highest temperature as FA exhibited a lower hydration rate than cement and slower pozzolanic reaction compared to SF. The F tests demonstrate the overall adequacy of both models as the p-values are very small.

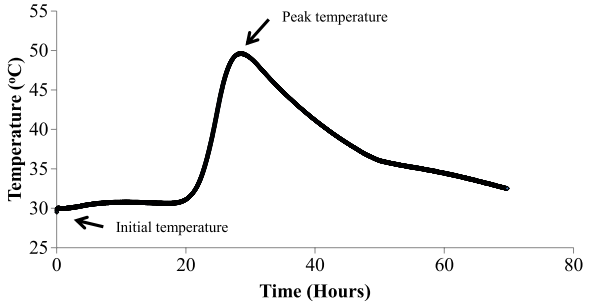

Fig. 7 Temperature curve from the semi-adiabatic test.

In terms of the T test, the p-value less than 0.05 is the criterion to gauge the significance of the regression coefficients. Based on that, the regression analysis of temperature rise (see Table 6) contains two significant variables (binder and FA + SF); the coefficient of SF is not significantly different from "0" with a 95% confidence interval ranging from −0.0375 to 0.1541 (°C/%). Therefore, the multiple linear regression model of temperature rise is not reliable. For the regression analysis of time to reach peak temperature (see Table 7), it contains only one significant variable (SF). Table 7 shows that the 95% confidence intervals of the coefficients of binder and FA + SF are from −0.1484 to 0.1023 (h/kg/m^3) and from −0.2862 to 0.7164 (h/%), respectively. These two intervals contain the value of "0"; therefore, the multiple linear regression model of duration to reach peak temperature is also unreliable.

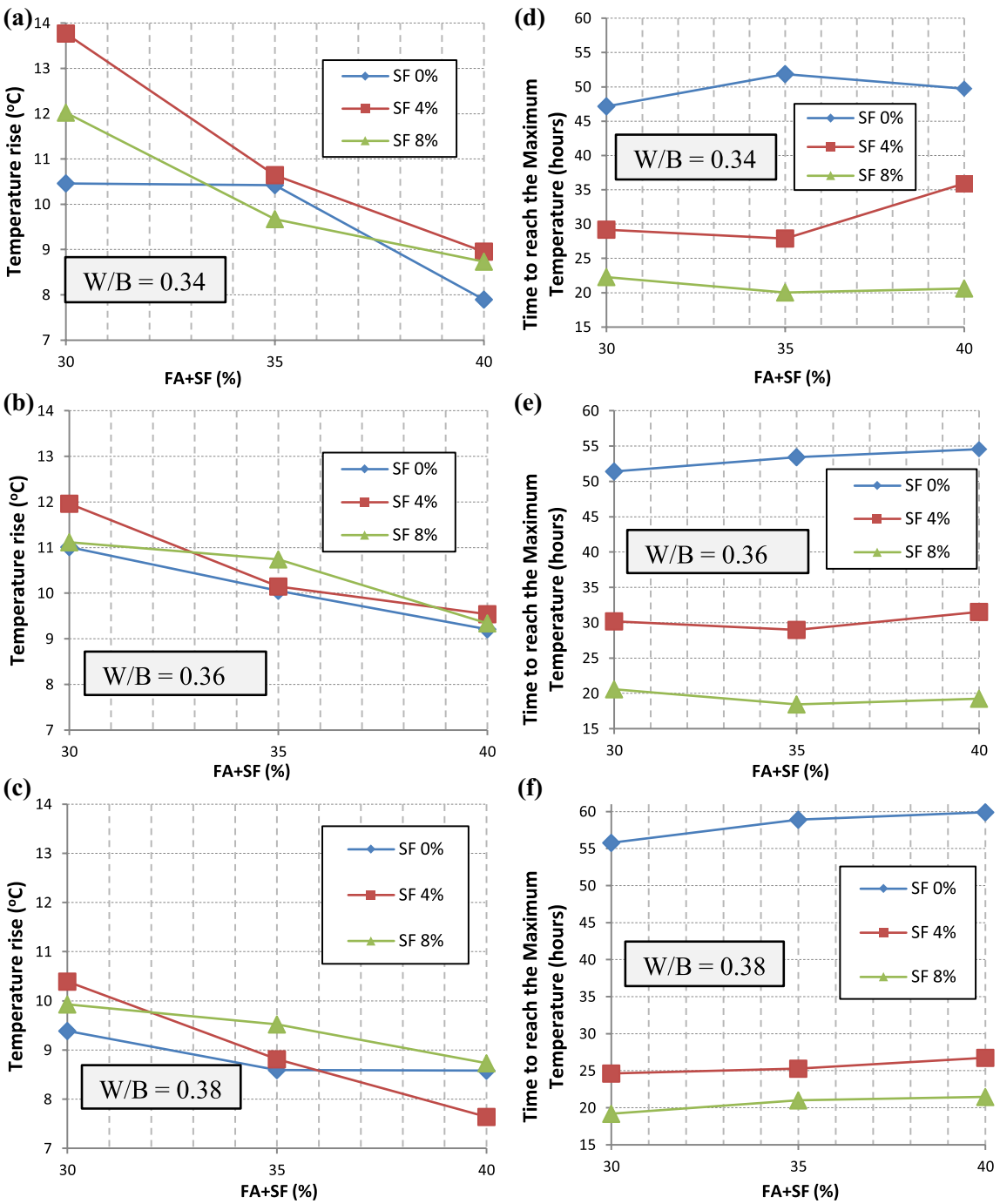

Fig. 8 Semi-adiabatic test results (**a**–**c** temperature rise of the concrete mixtures, **d**–**f** time to reach the peak temperature rise of the concrete mixtures).

3.2 Regression Analysis Results of Compressive Strength

Based on the regression analysis result of compressive strength (see Tables 8 and 9), compressive strength models were built and are presented as below:

$$f_{cu} = -66.938 + 0.330556M_{\text{binder}} - 0.86\text{P}_{\text{FA+SF}} + 1.454167P_{\text{SF}} \quad (7-\text{day}), \tag{3}$$

Table 6 Results of linear regression analysis on temperature rise's test.

***P*-value (F test): 3.22E(-6)** **Sample multiple coefficient of determination: $R^2 = 0.70$**			
	***y*-intercept (β_o) and the linear regression coefficients (β_1, β_2, β_3)**	***p*-value**	**95% of confidence interval**
y-intercept	5.48 (°C)	0.187	(− 2.8555; 13.8125)
Binder	0.030 (°C/kg/m^3)	0.0032	(0.0113; 0.0496)
FA + SF	− 0.238 (°C/%)	1.46E(-6)	(− 0.3149; − 0.1616)
SF	0.058 (°C/%)	0.22045	(− 0.0375; 0.1541)

Table 7 Results of linear regression analysis on time to reach peak temperature.

***P*-value (F test): 2.87E(−11)** **Sample multiple coefficient of determination: $R^2 = 0.89$**			
	y-intercept (β_o) and the linear regression coefficients (β_1, β_2, β_3)	***P*-value**	**95% of confidence interval**
y-intercept	52.89 (h)	0.0566	(− 1.6211; 107.4066)
Binder	− 0.023 (h/kg/m^3)	0.7073	(− 0.1484; 0.1023)
FA + SF	0.215 (h/%)	0.3839	(− 0.2862; 0.7164)
SF	− 4.165 (h/%)	1.4E−12	(− 4.7916; − 3.5383)

Table 8 Regression analysis of 7-day compressive strength.

***P*-value (F test): 4.09E(-11)** **Sample multiple coefficient of determination: $R^2 = 0.89$**			
	***y*-intercept (β_o) and the linear regression coefficients (β_1, β_2, β_3)**	***P*-value**	**95% of confidence interval**
y-intercept	− 66.938 (MPa)	0.0003	(− 99.486; − 34.390)
Binder	0.330556 (MPa/kg/m^3)	4.07E(−9)	(0.256; 0.405)
FA + SF	− 0.86 (MPa/%)	4.65E(−6)	(− 1.159; − 0.561)
SF	1.454167 (MPa/%)	3.94E(−8)	(1.080; 1.828)

Table 9 Regression analysis of 28-day compressive strength.

***P*-value (F test): 9.91E(−10)** **Sample multiple coefficient of determination: $R^2 = 0.85$**			
	***y*-intercept (β_o) and the linear regression coefficients (β_1, β_2, β_3)**	***P*-value**	**95% of confidence interval**
y-intercept	− 29.275 (MPa)	0.089	(− 63.368; 4.818)
Binder	0.275 (MPa/kg/m^3)	2.19E(−7)	(0.197; 0.353)
FA + SF	− 0.93778 (MPa/%)	2.59E(−6)	(− 1.251; − 0.624)
SF	1.231944 (MPa/%)	1.23E(−6)	(0.840; 1.624)

$$f_{\mathrm{cu}} = -29.275 + 0.275M_{\mathrm{binder}} - 0.93778P_{\mathrm{FA+SF}} + 1.231944P_{\mathrm{SF}} \quad (28-\mathrm{day}), \tag{4}$$

where f_{cu} is the outcome compressive strength (MPa), M_{binder} is the mass of total cementitious materials (from 431 kg/m^3 to 391 kg/m^3), $P_{\mathrm{FA+SF}}$ is the proportion of FA and SF (from 30 to 40%), which replaced cement (by mass), and P_{SF} is the proportion of SF (from 0 to 8%), which replaced cement (by mass). The remaining parameters in the equations are the y-intercept (β_o) and the linear regression coefficients (β_i), whose units can be found in Tables 8 and 9.

The overall adequacy of the models is satisfied as the p-values of F tests are significantly less than 0.05. All the independent variables are statistically significant as the *p*-values in T tests are smaller than 0.05, which means the 95% of confidence interval of each linear regression coefficient (β_i) will not contain the value of "0". In the domain investigation, binder content (kg/m^3) and the percentage of SF (%) show a positive effect on the concrete compressive strength of 7 days and 28 days. Every 1-unit increase in SF increases the concrete compressive strength of 7 days and 28 days to 1.45 MPa and 1.23 MPa. Meanwhile, for every 1-unit increase in the binder content, it increases the compressive strength of 7 days and 28 days to 0.33 MPa and 0.27 MPa, respectively. The "FA + SF" independent variable negatively affects the results of compressive strength of 7 days and 28 days, which reduces the compressive strength of 7 days and 28 days to 0.86 MPa and 0.94 MPa for every unit increment.

The validation of the model is assessed by the properties of the error term (ε) that are described in the assumptions in Sect. 2.2. However, the error term is generally unobservable. So instead, the next best thing closely related to the error term, the residual, is used to check the assumptions. Techniques to diagnose the violations of these assumptions are varied, including the graphical analyses of residuals or statistical tests. The former provides visual information of the residual plot, which is very useful and convenient, while the latter is more complicated with many equations for testing. Therefore, graphical analyses of the residuals are preferable and frequently used among papers published in analytical journals (Martin et al., 2017). To validate the compressive models, graphical analyses of residuals, which are presented in chapter 11.10 of the "*Statistics for engineering and the sciences*" (Mendenhall & Sincich, 2016), are conducted to check the assumptions of the error term.

Assumption 1—mean of residuals (ε) is "0", implies that the mean of the outcome is equivalent to the deterministic component of the model. Basically, the y-intercept (β_o) in the model will force the mean of residuals (ε) to equal "0". But if multiple linear regression is applied to the nonlinearly related data, it will violate this assumption of linearity, and the predictions are unlikely to be correct. The nonlinearity is usually most evident by examining the residual plots. Fig. 9 plots the residual (*y*-axis) against each of the three independent variables in the models (*x*-axis). If linear regression models are appropriate for the data, the points in Fig. 9 will be randomly dispersed around the *x*-axis; otherwise, the model is misspecified. Patterns observed in Fig. 9 do not show any systematic trend (e.g., curvilinear trend), and the points

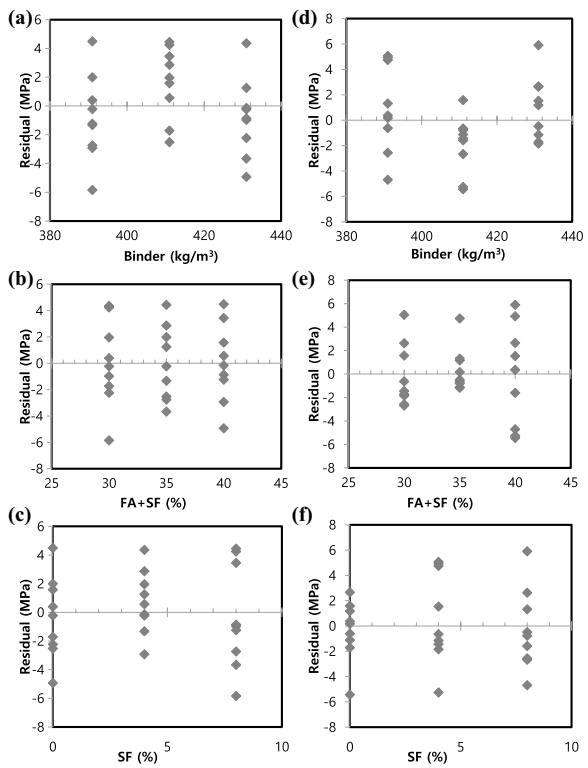

Fig. 9 Residual plots for checking assumption 1 (**a**–**c** residual versus independent variables in 7-day compressive strength model, **c**–**f** residual versus independent variables in 28-day compressive strength model).

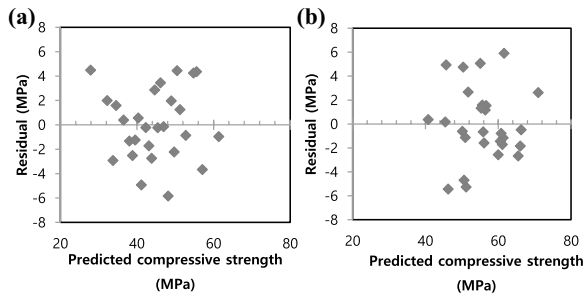

Fig. 10 Residual plots for checking assumption 2 (**a** residual versus predicted compressive strength in 7-day compressive strength model, **b** residual versus predicted compressive strength in 28-day compressive strength model).

are randomly dispersed. Therefore, the first assumption in compressive strength models is reasonably satisfied. The linearity of the model can also be checked by observing the plots of residuals versus predicted values (Fig. 10). The first assumption is reassured as the points in Fig. 10 are symmetrically distributed around the x-axis with a roughly constant variance.

In regression analysis, the least-squares method is applied to estimate the β_0 and β_i to produce the regression line with the minimum sum of squares for errors. The regression analysis works under the assumption of homoscedasticity (assumption 2), or the variance of the errors is constant. This means that the distributions of ε should have the same amount of spread or variability; otherwise, the data will not be suitable to build the regression model, and the model must be improved. Assumption 2 will be violated if the residual gets larger or smaller as the predicted compressive strength moves from small to large, which creates a "funnel" or "megaphone" shape in the residual plots. By examining the residual plots in Fig. 10, the assumption of constant variance of the compressive strength models is reasonably satisfied as there is no evidence of "funnel" or "megaphone" shape.

Assumption 3 is the normal distribution of ε. Violation of this assumption poses problems for determining whether model coefficients are significantly different from "0" and for calculating confidence intervals because the calculation of confidence intervals and significance tests for coefficient are all based on this assumption. The best test for this assumption is to apply probability plots on the residuals. If the distribution is normal, the points should fall close to the diagonal reference line. As shown in Fig. 11, the residual falls nearly in the straight line with the normal distribution; hence, the third assumption is also reasonably satisfied.

Finally, assumption 4 (independent errors) is most likely satisfied as compressive strength data are not a time series. It can be concluded that models on compressive strength are deemed adequate and reliable.

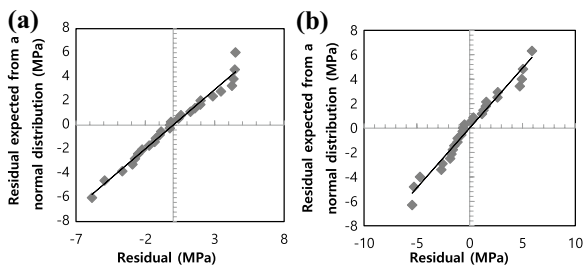

Fig. 11 Probability plots for checking assumption 3 (**a** probability plot of residual in 7-day compressive strength model, **b** probability plot of residual in 28-day compressive strength model).

3.3 Rapid Chloride Permeability Test Results

The RCPT is widely used for specification and quality control purposes. For example, in Canadian Standard (CSA A23.1:19, 2019), concrete mixture for the structure exposed to chlorides or other severe environments is required to have a W/B not exceed 0.4 and RCPT result not exceed 1000 coulombs within 91 days. According to the ASTM C1202 (2012), the areas above and below the value of 1000 coulombs indicate the low and very low chloride ion penetrability. As the turbine's slab foundation in this study is placed offshore, the project's construction specification required the 28-day RCPT results of the concrete mixture to be no more than 1000 coulombs. Fig. 12 also shows that the use of SF increased the chloride ion resistance of concrete, and the optimal incorporation of FA + SF in the mixture seemed to be 35%. For concrete with W/B = 0.34, the use of 4% and 8% SF ensured the very low chloride ion permeability requirement regardless of the variable FA + SF (%). Meanwhile, when the total binder was reduced (W/B = 0.36), there was only one SF value (8%) that could ensure the charge passed below 1000

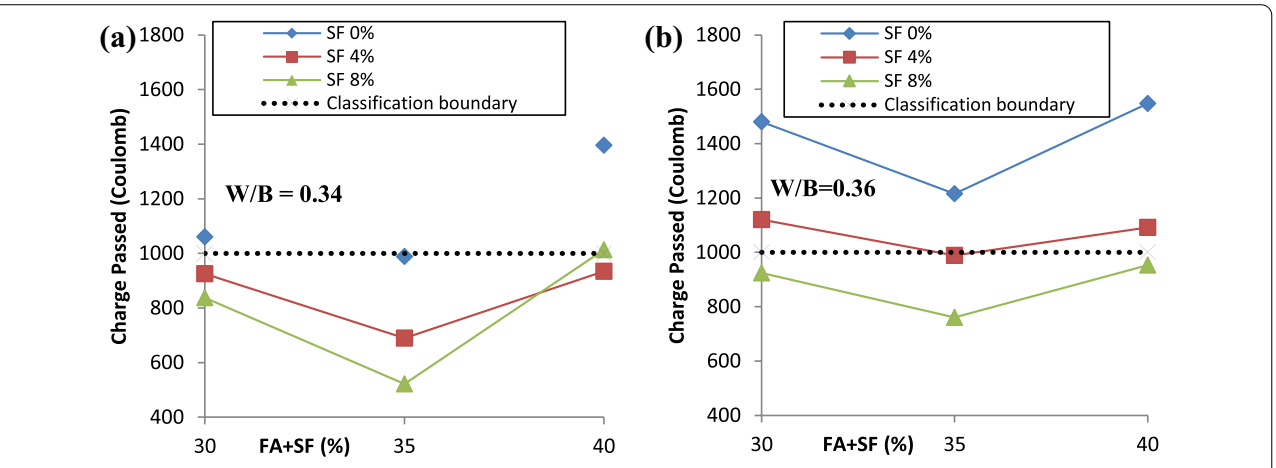

Fig. 12 RCPT results (**a** W/B = 0.34, **b** W/B = 0.36).

coulombs. The total binder of 391 kg/m^3 (highest W/B) was eliminated for this test because the high value of W/B increase the porosity of concrete (Rahmanzadeh et al., 2018).

3.4 Relationship Between the Results of Compressive Strength and Semi-adiabatic Peak Temperature

The development of concrete compressive strength is generally dependent on the function of hydration. Chemical reactions after mixing cement with water produce the hydration products that create bridges between material particles. As a result, the more hydration products being produced, the more compressive strength can be achieved. The volume of hydration products can be assessed by the linear relationship between the heat release and the early ages compressive strength (Lootens & Bentz, 2016).

Fig. 13 plots the compressive strength versus peak temperature in the semi-adiabatic test. The coefficient of determination ($R^2 = 0.73$) in Fig. 13a shows that 73% of the variation among the values of peak temperature is accounted for by the differences in 7-day compressive strength. This value is clearly higher than that of the relationship in Fig. 13b. The straight-line slope ($\beta_1 = 0.1521$) in Fig. 13a interprets that every 1-MPa increase in the 7-day compressive strength will increase the result of the peak temperature in the semi-adiabatic test to 0.1521 °C. Regression analysis in EXCEL also provides the statistical test to check whether the straight-line slope in Fig. 13a is significantly different from "0". The p-value from the T-test is very small (1.53E−8), which rejects the null hypothesis and indicates that the 7-day compressive strength contributes information for the prediction of peak temperature in the semi-adiabatic test using a linear model.

3.5 Optimization Method for Concrete Mixture Proportion

The preceding sections had focused on modeling several critical concrete properties (e.g., compressive strength and semi-temperature increase) as functions of total binder content and proportions of SCMs, and statistically assessed the reliability of these models. This section describes a detailed procedure for determining the optimum amount of binder and SCMs percentages that will benefit the placement of a huge offshore wind turbine foundation. Fig. 14 depicts the optimization process, which is defined as a computational optimization

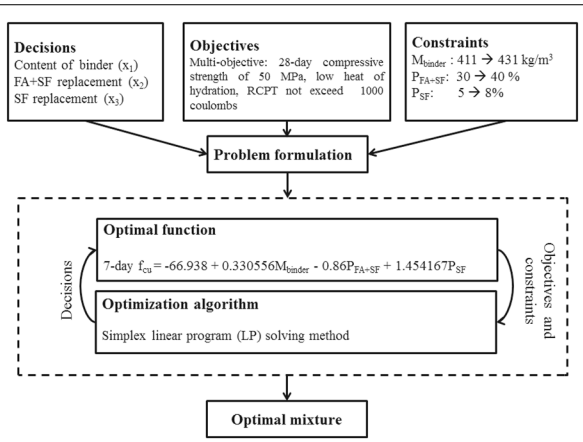

Fig. 14 Illustration of the optimization method.

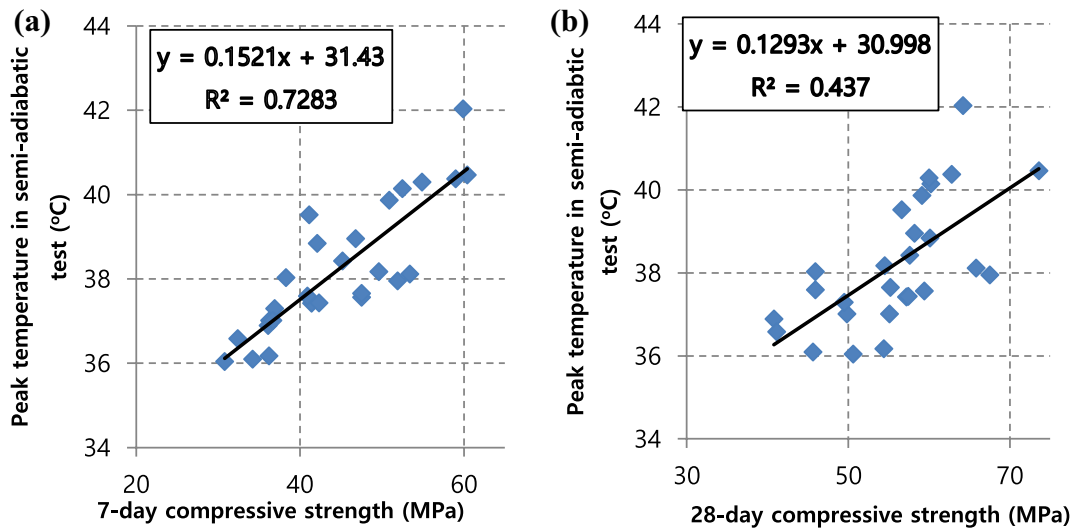

Fig. 13 Peak temperature in the semi-adiabatic test vs. Compressive strength value (**a** 7-day compressive strength, **b** 28-day compressive strength).

approach in DeRousseau et al., 2018. The approach can be recapitulated by explaining three main components: the problem formulation, optimal function, and the optimization algorithm.

Firstly, in the problem formulation, the specific decisions, objectives, and constraints are determined to represent the appropriate target of the concrete mixture design problem. The constituents, such as the binder, FA, and SF, were chosen as the decision variables because of their substantial impact on the performances of concrete (the compressive strength, the heat of hydration, and the resistance to chloride penetrability). Next, for the objectives, the tradeoffs should be assessed. For example, designing the concrete mixture to maximize the 28-day compressive strength while minimizing both the temperature rise in semi-adiabatic and the coulomb charge passed in RCPT seem impossible, at least in the context of this paper. Instead, it is more desirable to determine which level of compromise among the objectives. Therefore, the objectives would be a concrete mixture that satisfies the 28-day compressive strength of 50 MPa, low heat of hydration, and the stipulation of coulomb rating in RCPT not over 1000 at 28 days. Finally, the constraints establish a limit on decisions or objectives. For example, the limits in the use of binder, FA + SF, and SF should be imposed so that the outcomes of the heat of hydration and the coulomb charge passed in RCPT are feasible for the project specification. Also, if the optimal function is a 28-day compressive strength model, a limit of 50 MPa will be set for the objective.

Secondly, the optimal function is a statistical model for predicting a particular objective. At this stage, the most prominent model is the 7-day compressive strength multiple linear regression model (Eq. 3); the model has demonstrated its overall adequacy, as shown in Sect. 3.2. Meanwhile, the multiple linear regression model of the semi-adiabatic tests is not significantly reliable; it is difficult to optimize the concrete mixture which generates the least heat of hydration. However, there is a valid conclusion drawn in Sect. 3.4 that a linear trend may exist between the peak temperature in semi-adiabatic and the 7-day compressive strength. Therefore, choosing the model of 7-day compressive strength as an objective function may benefit from estimating the peak temperature of the semi-adiabatic test.

At the final stage, the optimal function provides the information of objectives and constraints to the optimization algorithm. The optimization algorithm is chosen based on its propriety to solve the problem mathematically. As the optimal function is a linear function, the simplex linear program (LP) in EXCEL was employed as an algorithm to solve the objective and gave back the results of each decision variable. Details of constraints on the decisions and objective are presented below:

- M_{binder} was set to change from 411 kg/m^3 to 431 kg/m^3 because values under 411 kg/m^3 would increase the W/B, which makes the concrete structure less prominent in the performance of the permeability resistance in the marine environment
- P_{FA+SF} was kept from 30 to 40% for reducing the heat of hydration. According to the regression analysis of temperature rise (Table 6), every 1-increment in FA + SF from 30 to 40% can help minimize the temperature rise by 0.238 °C. The FA + SF is the independent variable whose regression coefficient is statistically significant to interpret and the result of semi-adiabatic temperature rise.
- P_{SF} was imposed to run from 5 to 8% for ensuring the test value of RCPT lies under 1000 coulombs
- The minimum value of 7-day compressive strength ensures the 28-day compressive strength to stay beyond 50 MPa.

The objective was to minimize the 7-day compressive strength because it reduces the temperature rise, as discussed in Sect. 3.4. However, the value of 7-day compressive strength should not be too low as 28-day compressive strength would be adversely affected. The experimental program showed that the 7-day compressive strength was averagely equal to 79% of the 28-day compressive strength. However, the ratio could increase up to 90% in the worst cases, especially for the mixtures using 8% SF in the W/B = 0.36 series. Therefore, the optimization process' objectives required all 28-day compressive strength values higher than 50 MPa (see Fig. 15).

The setting of the objective and constraints are displayed in the Solver function in EXCEL (Fig. 15). Using the simplex LP method in the Solver function of EXCEL to solve the optimal function, Eq. (3), the optimal mixture design is presented in Fig. 15, in which the total binder content, the incorporation of FA + SF, and SF were 411 kg/m^3, 36%, and 5%, respectively. Fig. 15 also shows that the minimum value of the empirical 7-day compressive strength was equal to 45 MPa, which ensures the 28-day compressive strength (in the worst scenario) equals 50 MPa. Verification tests were conducted on the optimal mixture and showed that the value of 28-day compressive strength was 54.5 MPa. The charge passed in the RCPT test was 945 coulombs, which means the concrete mixture is a very low permeability classification.

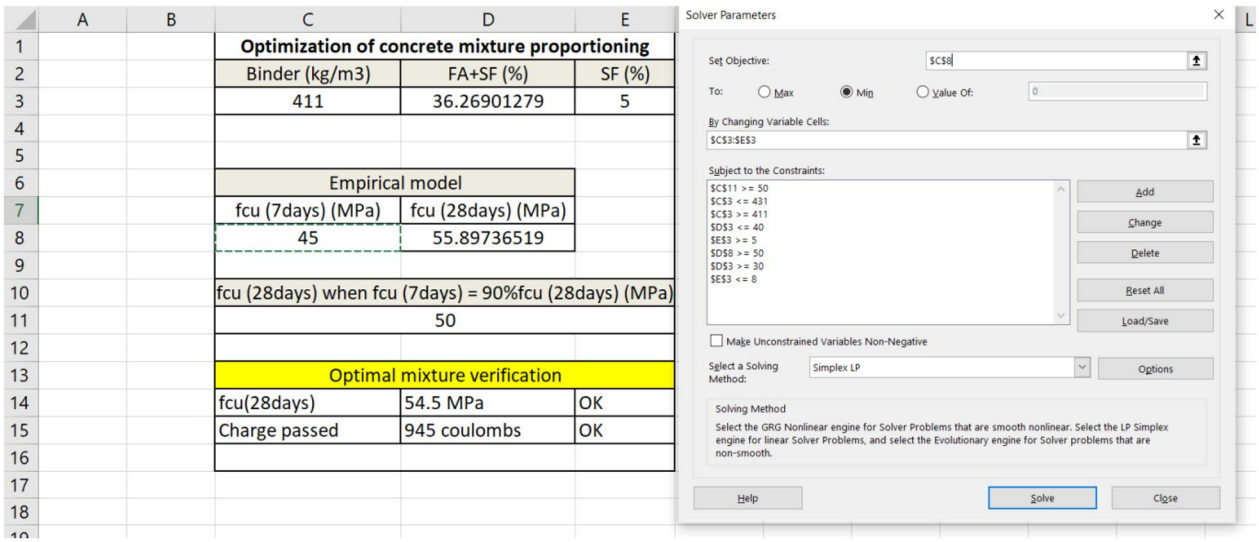

Fig. 15 Display of Solver function in EXCEL to optimize the concrete mixture proportion

Table 10 Concrete mixture proportion used for field testing.

Cement kg/m^3	FA kg/m^3 (%)	SF kg/m^3 (%)	Water kg/m^3	River sand kg/m^3	Crushed sand kg/m^3	Coarse aggregate kg/m^3	Superplasticizer liter/m^3
263.04	127.41 (31)	20.55 (5)	147.5	359	481	992	5.34

Binder = cement + FA + SF = 411 kg/m^3; FA + SF = 36% (by mass of Binder); SF = 5%(by mass of Binder).

4 Field Testing and Results

The optimum amount of binder and SCMs percentages obtained through an experimental program in the discussed section above was recommended for the actual mass placement of a wind turbine's concrete foundation. Table 10 shows the concrete mixture proportion given off by the concrete batching plant manufacturer. Overall, the optimal mixture in field testing contains the same amount of binder, FA, and SF as the optimal laboratory mixture. Also, the W/B of 0.36 and the same type and dosage of superplasticizer are maintained. Although the contents of fine and coarse aggregates are not required to strictly follow the optimal laboratory mixture, Table 10 shows that the amounts of individual aggregates are not significantly modified. Therefore, it could be concluded that the optimal mixture for field testing is identical to the optimal laboratory mixture.

There are several practical challenges that require the aggregate content to be slightly modified. To begin, even though the same types of aggregates were employed in both laboratory and field testing, differences in aggregate size distributions between laboratory and field testing were unavoidable. Furthermore, due to the difference in aggregate storage between the laboratory and the concrete batching plant, the operation of washing aggregates may be performed efficiently for aggregates used in the laboratory than those used in the field. Hence, the aggregates used to propose the optimal mixture in the laboratory contained less dust and clay than the aggregates used for field testing. Another factor was the difference in the mixing process. In the laboratory, the total volume of fresh concrete for one mixture was 40 L; this number is tiny in comparison to the volume of mixing concrete in the concrete mixer of the concrete batching plant, which was 2000 L. In addition, a gravity concrete mixer was used in the laboratory, whereas the concrete batching plant had a mixer with stronger mixing forces to deal with the enormous volume of mixing concrete. When the volume of mixing concrete is higher, some specifications, such as slump and compressive strength test, may be different than when the same mixture is mixed in a lower volume. That is why the concrete batching plant was allowed to modify the aggregate amount to meet the specification requirements.

When fresh concrete had been transported to the construction site, some tests were performed before placing concrete. Fresh concrete was poured into a wheelbarrow, then the temperature of concrete before placing was determined by a thermometer, and a concrete slump test was conducted. Following that, three concrete

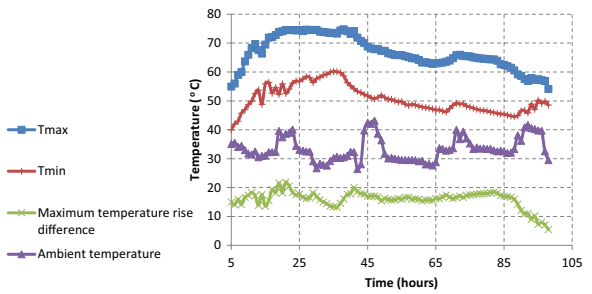

Fig. 16 Real-time monitoring of concrete mass placement.

cube samples were cast to verify the 28-day compressive strength, and three concrete cylinder samples were cast for the RCPT. The procedures for casting and curing these samples were identical to those used in the laboratory (Sect. 2.3). Finally, the fresh concrete was poured into the foundation's formwork by using two concrete pumps.

Fig. 16 shows the temperature rise of the wind turbine foundation's mass placement every 1-h interval time. During approximately 5 days of temperature rise monitoring, the maximum (T_{max}) and minimum temperature (T_{min}) rises were collected through the thermal sensors displayed in Fig. 6. Ambient temperature was also recorded. The results showed that the maximum temperature rise in the foundation reached 74.8 °C, and the maximum temperature differential was 21.9 °C. Both values satisfied the specifications of the proposal for constructing the foundation for an offshore wind turbine. However, the peak temperature rise nearly reached the maximum allowable temperature in the project specification (75 °C). The ambient temperature fluctuated from 28 °C at night to beyond 40 °C at noon. The maximum temperature difference significantly reduced after 85 h.

5 Conclusions

This study proposed a method that can be helpful to study the mass concrete mixture proportion from the laboratory point of view. By investigating and analyzing the effect of FA and SF replacing OPC on concrete's compressive strength, temperature rise in semi-adiabatic condition, and the RCPT, the optimal mixture was found to sufficiently satisfy the multi-objective problem: 28-day compressive strength of 50 MPa, low heat of hydration, and a specified maximum 1000 coulombs passed at 28 days. Based on the experimental results, the following conclusions could be drawn:

1. When FA + SF ranges from 30 to 40% as cement replacement and other independent variables are held fixed, the semi-adiabatic temperature rise reduces 0.238 °C for every 1% increase in FA + SF. When SF ranges from 0 to 8% as cement replacement and other independent variables are held fixed, the time to reach peak temperature reduces 4.165 h for every 1% increase in SF. Both parameters above were reliable since these p-values were very small. However, the semi-adiabatic test results (temperature rise and time to reach peak temperature) were not adequately fitted with the first-order multiple linear regression models because other variables were unreliable in multiple linear regression analysis (p-values were greater than 0.05).
2. The SF investigated in this experimental program shows a contradictory effect on the semi-adiabatic temperature rise results. Some mixtures with 4% SF result in a higher semi-adiabatic temperature rise than the mixtures with 8% SF.
3. The 7-day and 28-day compressive strength test results were adequately fitted with the first-order multiple linear regression models and were reliable because the p-values from F tests (to check the overall adequacy of models) and T tests (to examine the statistical significance of independent variables) are very small (lower than 0.05). When FA + SF ranges from 30 to 40% and other variables are held fixed, the 7-day and 28-day compressive strength reduce for every 1% increase in FA + SF. In contrast, every 1-unit increase in the binder (from 391 to 431 kg/m^3) or SF (from 0 to 8%) increases the 7-day and 28-day concrete compressive strength.
4. RCPT results showed that the optimal proportion of FA + SF is 35%, the increase of SF content significantly reduces the total charge passed.
5. The proposed method found that the optimal mixture should have 411 kg/m^3 of binder, 31% FA, and 5% SF (by mass of binder). The optimal mixture is practically useful to apply in the actual mass concrete pouring project since it contributed to preventing thermal damages and enhancing the durability of concrete in the marine environment.

Acknowledgements
We acknowledge the support of time and facilities from Ho Chi Minh City University of Technology (HCMUT), VNU-HCM for this study.

Authors' contributions
VNC: investigation, formal analysis, writing—original draft. MVT: conceptualization, methodology, writing—review and editing. All authors read and approved the final manuscript.

Authors' information
Mien V. Tran is an Associate Professor at the Faculty of Civil Engineering, Ho Chi Minh City University of Technology (HCMUT), Vietnam National University Ho Chi Minh City, Vietnam.

Vinh N. Chau is a graduate student of the Faculty of Civil Engineering, Ho Chi Minh City University of Technology (HCMUT), Vietnam National University Ho Chi Minh City, Vietnam.

Funding
This research received no external funding.

Availability of data and materials
The datasets used and/or analyzed during the current study are available from the corresponding author on reasonable request.

Declarations

Competing interests
The authors declare that they have no competing interests.

Author details
[1]Faculty of Civil Engineering, Ho Chi Minh City University of Technology (HCMUT), 268 Ly Thuong Kiet Street, District 10, Ho Chi Minh City 70000, Vietnam. [2]Vietnam National University Ho Chi Minh City, Linh Trung Ward, Thu Duc District, Ho Chi Minh City 70000, Vietnam.

Received: 18 April 2021 Accepted: 9 December 2021
Published online: 20 December 2021

References

ACI 234R-06. (2006). Guide for the Use of Silica Fume in Concrete, American Concrete Institute, Farmington Hills, MI, USA.
ASTM C1202-12. (2012). Standard Test Method for Electrical Indication of Concrete's Ability to Resist Chloride Ion Penetration, ASTM International, West Conshohocken, PA.
ASTM C618-12a. (2012). Standard Specification for Coal Fly Ash and Raw or Calcined Natural Pozzolan for Use in Concrete, ASTM International, West Conshohocken, PA.
Bentz, D. P. (2000). Influence of Silica Fume on Diffusivity in Cement-Based Materials II. Multi-Scale Modeling of Concrete Diffusivity, *Cement and Concrete Research*, [online], https://tsapps.nist.gov/publication/get_pdf.cfm?pub_id=860225 (Accessed June 8, 2021)
Berndt, M. L. (2004). Sustainable concrete for wind turbine foundations. *Brookhaven National Laboratory (US)*. https://doi.org/10.2172/15008841
Bofang, Z. (2014). *Thermal stresses and temperature control of mass concrete*. Butterworth Heinemann.
Boğa, A. R., & Topçu, İB. (2012). Influence of fly ash on corrosion resistance and chloride ion permeability of concrete. *Construction and Building Materials, 31*, 258–264. https://doi.org/10.1016/j.conbuildmat.2011.12.106
Chalee, W., Ausapanit, P., & Jaturapitakkul, C. (2010). Utilization of fly ash concrete in marine environment for long term design life analysis. *Materials & Design, 31*(3), 1242–1249. https://doi.org/10.1016/j.matdes.2009.09.024
Chau, V., Tran, M., & Dang, H. (2020). Experimental prediction of temperature rise of mass concrete basing on semi-adiabatic test. In: N. Banthia, K.Takewaka, C.Miao & H.Hamada (eds) Proceeding of the 6th International conference on construction materials: Performance, Innovations, and Structural Implications, Fukuoka, Japan, 2020.
Chu, T. X. H., Zheng, J., Chen, D., Nguyen, T. T. H., Elbashiry, E., & Tang, V. T. (2019). Utilization of industrial waste in cement in a marine environment with a tropical climate. *Journal of Marine Science and Engineering, 7*(8), 245. https://doi.org/10.3390/jmse7080245
CSA A23.1:19/CSA A23.2:19. (2019). Concrete materials and methods of concrete construction/Test methods and standard practices for concrete, Canadian Standards Association
DeRousseau, M. A., Kasprzyk, J. R., & Srubar, W. V. (2018). Computational design optimization of concrete mixtures: A review. *Cement and Concrete Research, 109*, 42–53. https://doi.org/10.1016/j.cemconres.2018.04.007
Durán-Herrera, A., Juárez, C. A., Valdez, P., & Bentz, D. P. (2011). Evaluation of sustainable high-volume fly ash concretes. *Cement and Concrete Composites, 33*(1), 39–45. https://doi.org/10.1016/j.cemconcomp.2010.09.020
Gesoğlu, M., Güneyisi, E., & Özbay, E. (2009). Properties of self-compacting concretes made with binary, ternary, and quaternary cementitious blends of fly ash, blast furnace slag, and silica fume. *Construction and Building Materials, 23*(5), 1847–1854. https://doi.org/10.1016/j.conbuildmat.2008.09.015
Ghosh, P., & Tran, Q. (2015). Correlation between bulk and surface resistivity of concrete. *International Journal of Concrete Structures Materials, 9*, 119–132. https://doi.org/10.1007/s40069-014-0094-z
Holland, R. B., Kurtis, K. E., & Kahn, L.F. (2016). 7 - Effect of different concrete materials on the corrosion of the embedded reinforcing steel, in Amir Poursaee (ed), *Corrosion of Steel in Concrete Structures*, Woodhead Publishing, 131–147, https://doi.org/10.1016/B978-1-78242-381-2.00007-9
Imam, A., Kumar, V., & Srivastava, V. (2018). Review study towards effect of Silica Fume on the fresh and hardened properties of concrete. *Advances in Concrete Construction., 6*, 145–157. https://doi.org/10.12989/acc.2018.6.2.145
Kadri, E. H., & Duval, R. (2009). Hydration heat kinetics of concrete with silica fume. *Construction and Building Materials, 23*(11), 3388–3392. https://doi.org/10.1016/j.conbuildmat.2009.06.008
Lee, J. W., Bae, J. Y., Jang, Y. I., & Lee, B. J. (2018). Study on estimation of concrete adiabatic temperature rise coefficient by using mortar semi-adiabatic temperature rise test. *International Journal of Civil Engineering and Technology (IJCIET), 9*, 1351–1359.
Leung, H. Y., Kim, J., Nadeem, A., Jaganathan, J., & Anwar, M. P. (2016). Sorptivity of self-compacting concrete containing fly ash and silica fume. *Construction and Building Materials, 113*, 369–375. https://doi.org/10.1016/j.conbuildmat.2016.03.071
Li, G. (2004). Properties of high-volume fly ash concrete incorporating nano-SiO2. *Cement and Concrete Research, 34*(6), 1043–1049. https://doi.org/10.1016/j.cemconres.2003.11.013
Lootens, D., & Bentz, D. P. (2016). On the relation of setting and early-age strength development to porosity and hydration in cement-based materials. *Cement & Concrete Composites, 68*, 9–14. https://doi.org/10.1016/j.cemconcomp.2016.02.010
Martin, J., Adana, D., & Garcia Asuero, A. (2017). Fitting Models to Data: Residual Analysis, a Primer, *In book: Uncertainty Quantification and Model Calibration*. http://dx.doi.org/https://doi.org/10.5772/68049
Martín-Pérez, B., Zibara, H., Hooton, R. D., & Thomas, M. D. A. (2000). A study of the effect of chloride binding on service life predictions. *Cement and Concrete Research, 30*(8), 1215–1223. https://doi.org/10.1016/S0008-8846(00)00339-2
Mendenhall, W. M., & Sincich, T. L. (2016). Statistics for engineering and the sciences. Chapman and Hall/CRC. https://doi.org/10.1201/b19628
Mitani, Y., Ohno, T., & Tada, K. (2016). Physical properties and thermal cracking risk of concrete using fly ash cement under the Southeast Asia environment. In: Proceeding of the 7th International Conference of Asian Concrete Federation: "Sustainable concrete for now and the future", Hanoi, Vietnam, 2016
Neville, A. M. (1997). *Properties of Concrete* (4th ed.). Addison Wesley Longman Limited.
Pedersen, K. H., Jensen, A. D., Skjøth-Rasmussen, M. S., & Dam-Johansen, K. (2008). A review of the interference of carbon containing fly ash with air entrainment in concrete. *Progress in Energy and Combustion Science, 34*(2), 135–154. https://doi.org/10.1016/j.pecs.2007.03.002
Poon, C. S., Lam, L., & Wong, Y. L. (2000). A study on high strength concrete prepared with large volumes of low calcium fly ash. *Cement and Concrete Research, 30*(3), 447–455. https://doi.org/10.1016/S0008-8846(99)00271-9
Rahmanzadeh, B., Rahmani, K., & Piroti, S. (2018). Experimental study of the effect of water-cement ratio on compressive strength, abrasion resistance, porosity and permeability of Nano silica concrete. *Frattura Ed Integrità Strutturale, 12*(44), 16–24. https://doi.org/10.3221/IGF-ESIS.44.02
Rashad, A. M. (2015). A brief on high-volume Class F fly ash as cement replacement—A guide for Civil Engineer. *International Journal of Sustainable Built Environment, 4*(2), 278–306. https://doi.org/10.1016/j.ijsbe.2015.10.002
Riding, K. A., Poole, J. L., Schindler, A. K., Juenger, M. C. G., & Folliard, K. J. (2006). Evaluation of temperature prediction methods for mass concrete members. *ACI Materials Journal*. https://doi.org/10.14359/18158
Santhanam, M., & Otieno, M. (2016). Marine Concrete Structures. Part Two: The performance and properties of concrete in the marine environment, 137–149. https://doi.org/10.1016/B978-0-08-100081-6.00005-2
Shaikh, F., Kerai, S., & Kerai, S. (2015). Effect of micro-silica on mechanical and durability properties of high volume fly ash recycled aggregate concretes

(HVFA-RAC). *Advances in concrete construction, 3*(4), 317–331. https://doi.org/10.12989/acc.2015.3.4.317
Tada, K., Lim, J., Doraipandian, L., Mitani, Y., & Ohno, T. (2016). Study for practical use of fly ash in mass concrete structure in Singapore. In: Proceeding of the 7th International Conference of Asian Concrete Federation: "Sustainable concrete for now and the future", Hanoi, Vietnam, 2016
TCE1: Adiabatic and semi-adiabatic calorimetry to determine the temperature increase in concrete due to hydration heat of the cement. (1997). *Materials and Structures*, 30(8), 451–464. https://doi.org/10.1007/BF02524773
TCVN 10302. (2014). Activity admixture - Fly ash for concrete, mortar and cement. Ministry of Science and Technology. Vietnam.
TCVN 7572. (2006). Aggregates for concrete and mortar – Test methods. Ministry of Science and Technology. Vietnam.
Thomas, M (2016), 6-The durability of concrete for marine construction: Materials and properties. In: Alexander MG (ed). *Marine concrete structures: design, durability and performance*, Woodhead Publishing, pp.151–170, doi:https://doi.org/10.1016/B978-0-08-100081-6.00006-4.
Thomas, M. D. A., Hooton, R. D., Scott, A., & Zibara, H. (2012). The effect of supplementary cementitious materials on chloride binding in hardened cement paste. *Cement and Concrete Research, 42*(1), 1–7. https://doi.org/10.1016/j.cemconres.2011.01.001
Weng, J. K., Langan, B. W., & Ward, M. A. (1997). Pozzolanic reaction in portland cement, silica fume, and fly ash mixtures. *Canadian Journal of Civil Engineering., 24*(5), 754–760. https://doi.org/10.1139/l97-025
Yoshitake, I., Komure, H., Nassif, A. Y., & Fukumoto, S. (2013). Tensile properties of high volume fly-ash (HVFA) concrete with limestone aggregate. *Construction and Building Materials, 49*, 101–109. https://doi.org/10.1016/j.conbuildmat.2013.08.020

Publisher's Note